

Planar Beam-Scanning Microstrip Antenna Using Tunable Reactance Devices for Satellite Communication Mobile Terminal

Naoki Honma[†], Tomohiro Seki, and Koichi Tsunekawa

Abstract

A series-fed beam-scanning array using a multi-stage configured microstrip antenna with tunable reactance devices (MUSCAT) for satellite communication mobile terminals is proposed. This antenna significantly expands the beam scanning range and achieves high efficiency. It comprises unit element groups, whose elements are placed close to each other and use tunable reactance devices. Analyses and experiments on the unit element groups showed that their multi-stage configuration extends the phase shift range and increases the radiation efficiency (e.g., a phase shift of 120° and radiation efficiency of more than 50%) when three stages are used. The radiation pattern of a fabricated MUSCAT array antenna with eight unit element groups was measured. The beam scanning range was 27° , which is more than twice that of a non-multi-stage configuration.

1. Introduction

A mobile satellite communication system can be used to provide geographically seamless communication service even in a rural area without an infrastructure [1], [2]. Since this system requires terminal antennas with high actual gain to obtain a high data rate for downlink transmission, the mobile terminal must constantly direct its beam toward the satellite. To provide such satellite communication services for a mobile vehicle, which may move at high speed, we must use a low-profile satellite-tracking antenna for aerodynamic reasons.

The combination of a one-dimensional planar phased array antenna and a rotator for azimuth control is one feasible solution. However, the configuration and control of the phased array antenna is complicated even for one-dimensional beam scanning because a lot of phase shifters are employed. Moreover, each phase shifter needs a low-noise amplifier to compensate for the insertion loss of the phase shifter. This causes high power consumption.

A series-fed beam-scanning array antenna can simplify the control of the phase shifters because series-

fed circuits enable the antennas to scan the beam direction easily with only a single control signal for the phase shifters. In addition, the insertion loss due to conduction loss can be reduced because this antenna can have a short feedline. James et al. [3] reported an example of a planar beam-scanning antenna employing such a feed circuit and proposed a design for an antenna employing varactor diodes as tunable reactance devices inserted between the strip conductor and the ground plane. Since it uses a planar antenna on the substrate, all of the devices can be easily mounted on the substrate. This planar array antenna can be constructed compactly. The varactor diodes, themselves, consume little power because little current flows into a varactor with reverse DC-bias. When varactor diodes with low insertion resistance are used, there is no need to use many low-noise amplifiers. Although this antenna reduces the complexity and loss, the reactance of the devices must be changed significantly when wide-range scanning is required. In this case, the reflection power and loss at the devices accumulate in the series feedline, and these factors affect the radiation pattern. This problem reduces the beam-scanning angle.

In this paper, we propose a novel series-fed beam-scanning array antenna consisting of a multi-stage configured microstrip antenna with tunable reactance devices (MUSCAT). Each element group comprises

[†] NTT Network Innovation Laboratories
Yokosuka-shi, 239-0847 Japan
E-mail: honma.naoki@lab.ntt.co.jp

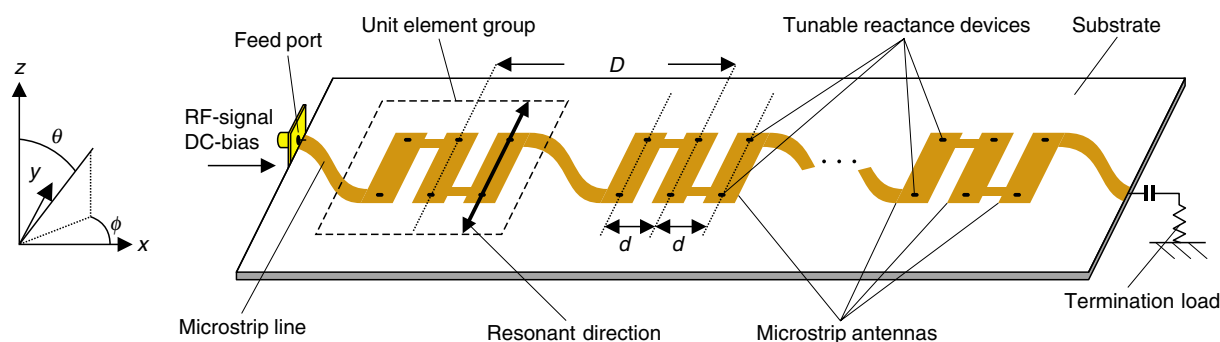


Fig. 1. Geometry of MUSCAT array antenna.

several microstrip antennas placed close together and uses tunable reactance devices. This provides a low-profile phased array antenna with a simple geometry and low-loss beam-scanning performance. Numerical and experimental results for the phase shift performance and radiation properties of the unit element group are presented. The beam scanning characteristics of a fabricated antenna with eight element groups are also shown to demonstrate wide-beam scanning and easy operation with low loss.

2. Geometry of MUSCAT array antenna

The geometry of the MUSCAT array antenna is shown in **Fig. 1**. Each element group is constructed of narrow microstrip antennas connected to each other by microstrip lines, where the element spacing d is much less than the wavelength in vacuum. The resonant direction of the narrow microstrip antenna is parallel to the long side of the rectangular antenna. The microstrip lines at both ends of the microstrip antenna are configured so as to cancel the undesired radiation generated by themselves. Two reactance devices, which can be tuned using DC-voltage, are attached to the ends of the microstrip antenna. **Figure 2** is a cross section of the MUSCAT array. The devices are connected to the microstrip antennas and the ground plane via through holes.

The MUSCAT array comprises several unit element groups and the spacing between neighboring groups denoted by D is much greater than element spacing d . All of the unit element groups have the same dimensions and are connected in series by microstrip lines having an 'S' shape to adjust the phases in the unit element groups. In this traveling wave array antenna, some of the power incident to one antenna element is radiated and the remaining power is delivered to the next element. Since the delay of the signal also propagates from one element to the next and accumulates

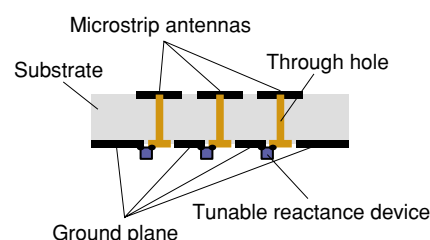


Fig. 2. Cross section of antenna.

through the series feedline, it is easy to provide a relatively large beam scanning range without employing 360° phase shifters. Furthermore, this antenna can provide large phase shifts in the unit element groups because these groups have a multi-stage configuration, and the unit element groups, which all have identical dimensions, achieve a phase front without distortion when all of the reactance devices are tuned to the same state. The termination load connected to the end of the array suppresses the reflection of the traveling wave, which causes undesired radiation [4], [5]. This geometry can control all the reactance devices with a single DC bias. The RF-signal and the DC bias are supplied through the same feedline. This mechanism simplifies the feed and bias network configuration and enables easy beam steering.

3. Properties of unit element group

The MUSCAT array has a series-fed configuration. However, the accumulated insertion loss and the reflection at the input port of the unit element group in the series array antenna cause a reduction in the actual gain and produce a backward traveling wave that generates undesired radiation. Moreover, many tunable reactance elements are used in the MUSCAT array and the power consumed by them is not negligible. For these reasons, it is necessary to investigate the radiation, reflection, and loss of the unit element

group in order to design the MUSCAT array.

To enable us to discuss the actual performance of the MUSCAT array, we measured the impedance of the varactor diodes. **Figure 3** shows the measured impedance of the varactor diode versus DC-bias voltage when a Renesas Technology HVU316 was used as the tunable reactance device and the operating frequency is 2.4 GHz. Since high absolute values for the reactance and low resistance are observed in the high voltage range, the bias voltage should be as high as possible so as to decrease the loss in the varactor diodes.

Based on these results, we investigated the scattering parameters of the unit element group numerically using the moment method [6] and experimentally. A model of the unit element group is shown in **Fig. 4**, where λ_0 is the wavelength in vacuum, m denotes the number of stages (i.e., the number of elements in the unit element group), the element spacing is $d = 0.12$

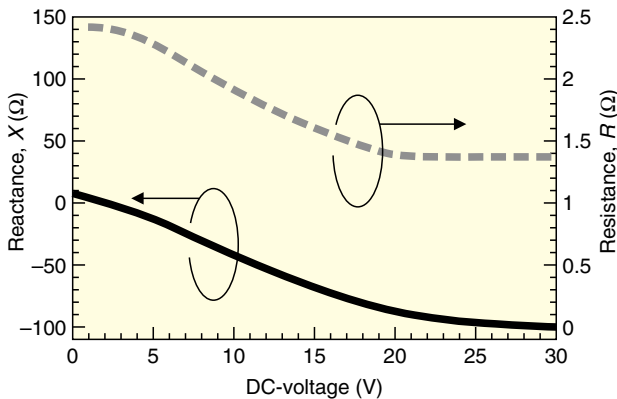


Fig. 3. Measured impedance of varactor diode versus DC-voltage.

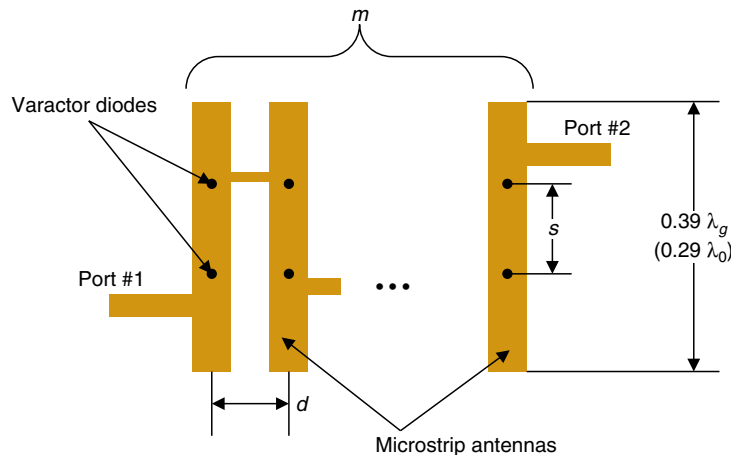


Fig. 4. Configuration of unit element group.

λ_0 , and the distance between two varactor diodes in the microstrip antennas is s . The thickness of the substrate is $0.02 \lambda_0$, and the relative dielectric constant is $\epsilon_r = 2.2$. The length of the microstrip antenna is $0.39 \lambda_g$ where λ_g is the effective wavelength in the microstrip antenna. The antenna length is obtained from the effective dielectric constant given in [7]. The operating frequency is 2.4 GHz.

3.1 Numerical analysis of radiation and phase shift performance in unit element group

We investigated the relationship between the number of elements m and the phase shift. The magnitude and phase of S_{21} obtained from the calculation for $m = 3$ are shown in **Fig. 5**. Here, the distance between two varactor diodes is set to $0.153 \lambda_g$. The $\Delta|S_{21}|$ and Φ are defined as the transmission power difference and phase difference from the reference S_{21} at 30 V, respectively. The Φ_{\max} is the Φ at the DC-voltage where the magnitude of S_{21} is 1 dB below the magnitude of S_{21} at 30 V.

The results shown in Fig. 5 indicate that the transmission power decreases as the DC-voltage decreases. This is due to the loss caused by the varactor diodes when the DC-voltage is low, as shown in Fig. 3.

Next, we investigated the relationship between spacing s of the two varactor diodes in the microstrip antenna and Φ_{\max} of the unit element group. The calculated phase shift performance of the unit element group is shown in **Fig. 6**. The characteristic impedance of the input or output feedline was optimized to obtain the largest Φ_{\max} , and the optimized value of the impedance Z_0 is shown in Fig. 6(b). There is a discontinuity in Z_0 around $0.16 \lambda_g < s < 0.17 \lambda_g$, which

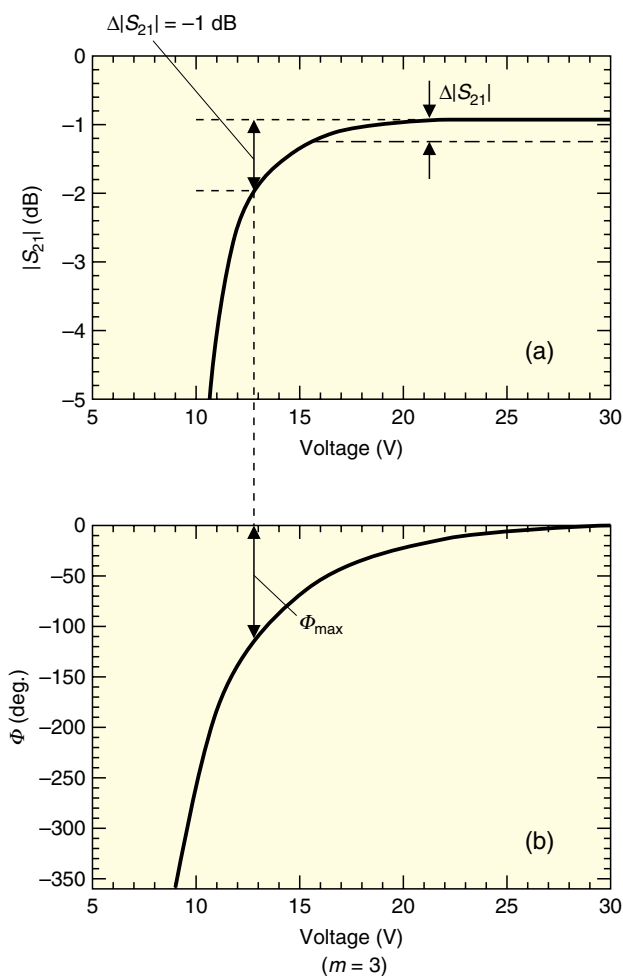


Fig. 5. Calculated $|S_{21}|$ and ϕ versus voltage: (a) $|S_{21}|$ and (b) ϕ .

corresponds to the distance between the two feedlines at the microstrip antenna. Considering this, we conjectured that this discontinuity is caused by the feedlines. The results in Fig. 6 show that the largest Φ_{\max} value is obtained for $s = 0.153 \lambda_g$. In the following discussion, this optimum distance is used.

Figure 7 shows the relationship between the number of elements m and the maximum phase shift Φ_{\max} obtained from the calculation. The Φ_{\max} increases almost linearly as m increases. This means that the effect of the mutual coupling between the elements in the multi-stage configuration of the unit element group has little effect on the phase shift performance.

To clarify the radiation performance in the unit element group, we must consider the transmission power because it is incident to the next unit element group and is radiated. In this paper, the radiation efficiency η_e of the unit element group is defined as

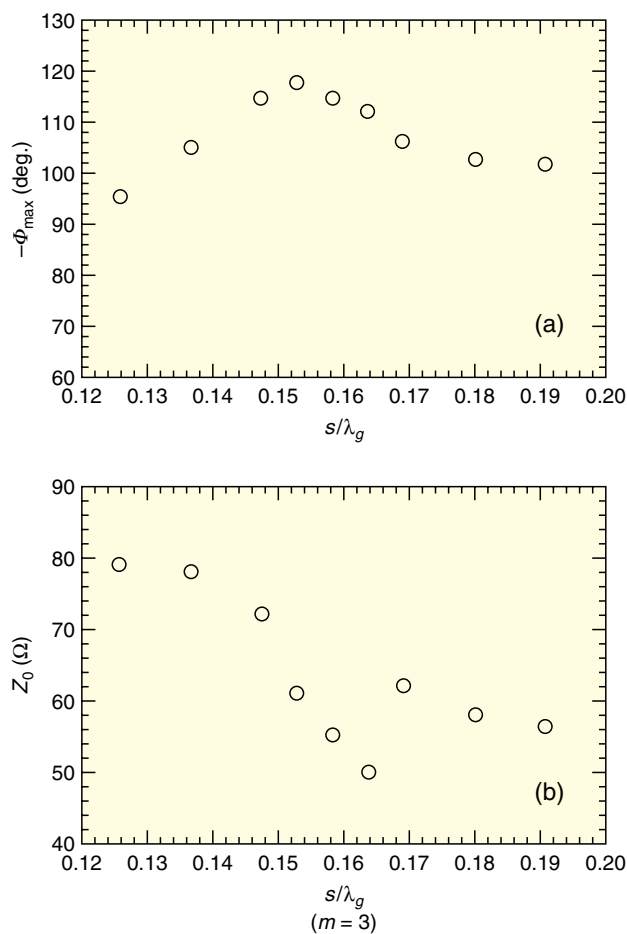


Fig. 6. Unit element group properties versus varactor diode distance s : (a) Φ_{\max} and (b) characteristic impedance of feedline Z_0 .

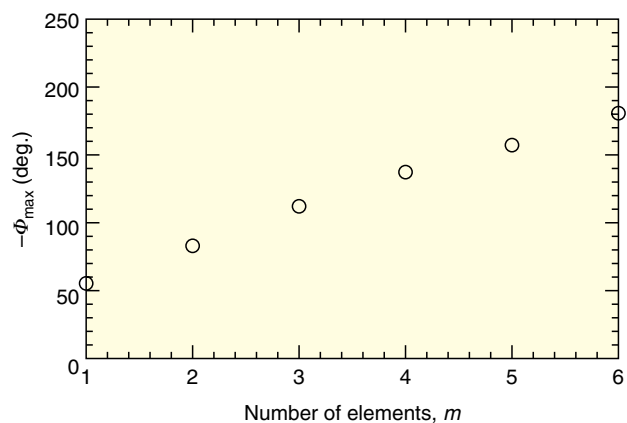


Fig. 7. Maximum phase shift Φ_{\max} versus number of elements m .

$$\eta_e = \frac{P_{rad}}{P_{inc}(1-|S_{21}|^2)}, \quad (1)$$

where P_{inc} is the incident power at input port #1 of one unit element group and P_{rad} is the radiation power of the unit element group. The calculated radiation efficiency of the unit element group obtained from Eq. (1) is shown in Fig. 8. Here, the average of the radiation efficiency is used for simplicity because η_e depends on the bias voltage. The $\bar{\eta}_e$ represents the averaged radiation efficiency and is defined by

$$\bar{\eta}_e = \int_0^{\Phi_{max}} \eta_e d\Phi / \Phi_{max}. \quad (2)$$

The results shown in Fig. 8 indicate that $\bar{\eta}_e$ increases with m . This is because the low loss range of the varactor diode is used in the unit element group with a large m . Thus, the proposed configuration can achieve both a large phase shift and a high level of radiation efficiency when the number of the elements is large.

In the following discussion, m is set to 3 so that the spacing between neighboring unit element groups is $D = 0.5 \lambda_0$, since the unit element groups with $m > 3$ require a D value larger than $0.5 \lambda_0$ and a grating lobe is generated when the beam of the MUSCAT array is steered. In addition, more than 50% of the average radiation efficiency $\bar{\eta}_e$ is obtained in the unit element group with $m = 3$ and the increase in the radiation efficiency is not so large when m is greater than 3.

The radiation pattern of a single unit element group with $m = 3$ is shown in Fig. 9. The radiation pattern of the unit element group is similar to that of a single microstrip antenna. This is because element spacing d is sufficiently small. A beam tilt to the right is obtained when the bias voltage is low. Figure 10

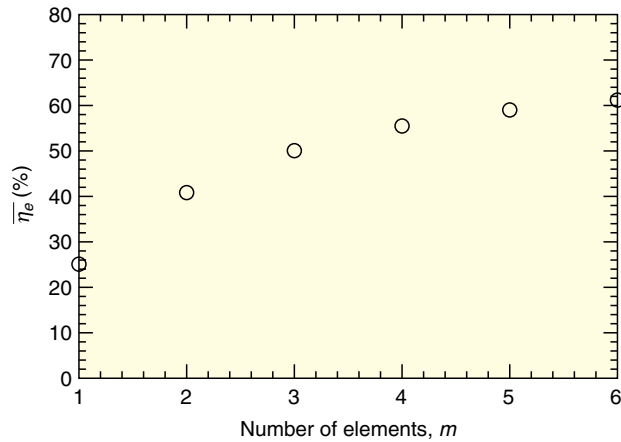


Fig. 8. Average radiation efficiency versus number of elements m .

shows the peak direction of the radiation pattern versus the bias voltage. The tilt direction is the same as the beam scanning direction of the array with several unit element groups, and this hardly affects the beam scanning performance of the MUSCAT array.

3.2 Measurement of scattering parameter in unit element group

To confirm the validity of the proposed configuration, we measured the scattering parameters of a fabricated unit element group with $m = 3$. For comparison, we calculated the properties of a unit element group with $m = 1$ and the conventional phase shifter

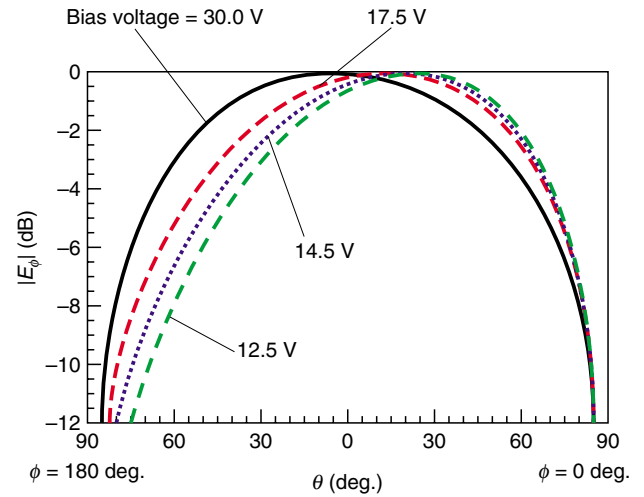


Fig. 9. Calculated radiation pattern of unit element group (zx -plane).

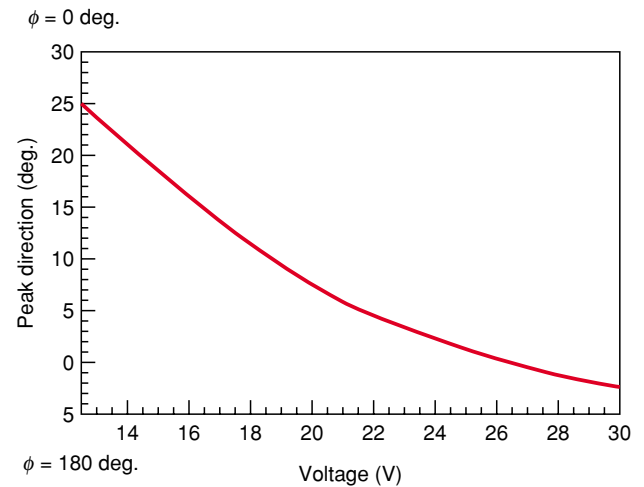


Fig. 10. Peak direction of unit element versus group bias voltage.

[3] shown in **Fig. 11(a)**. The conventional phase shifter comprised a microstrip line with a low characteristic impedance of less than 20Ω and a pair of varactor diodes located between the microstrip line and the ground plane. To alleviate the reflection, the distance between the varactor diodes is set to $\lambda_g/4$. This

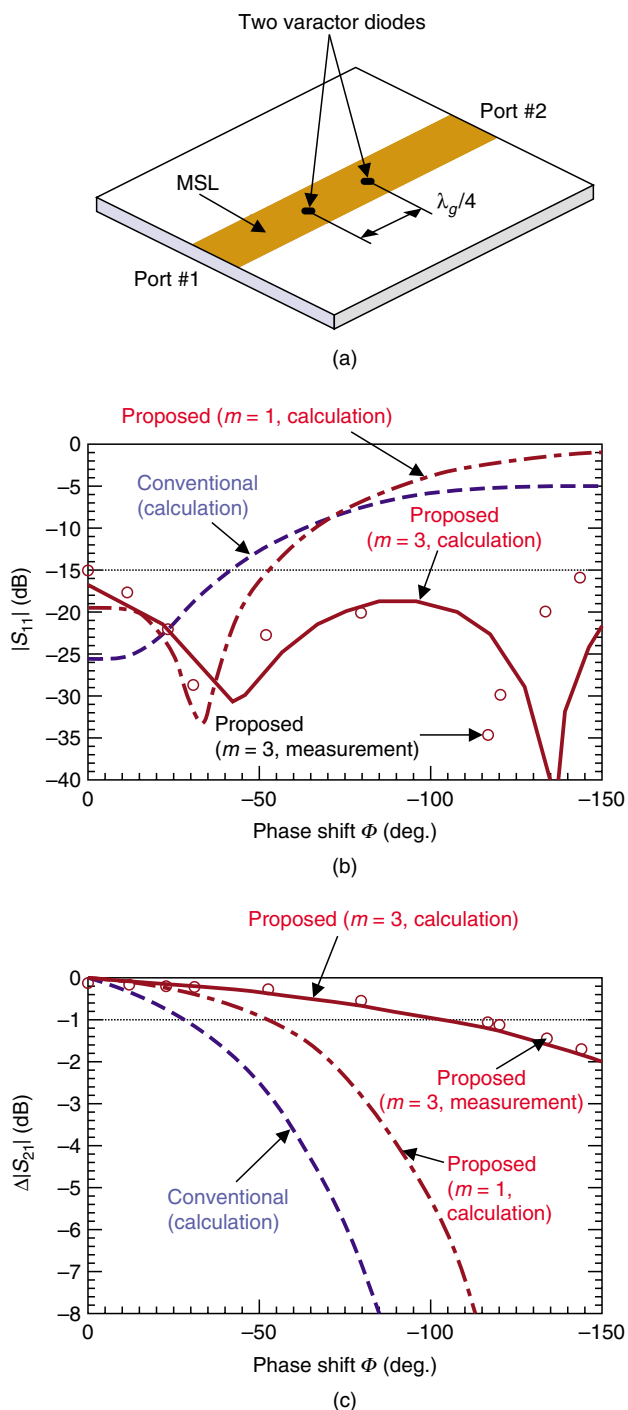


Fig. 11. $|S_{11}|$ and $\Delta|S_{21}|$ versus phase shift Φ in unit element group.

phase shifter is controlled by the DC-voltage applied to the microstrip line.

Figures 11(b) and **(c)** show the scattering parameters versus Φ . The results of measurements and numerical analysis for $m = 3$ indicate that the unit element group can provide a phase shift over 140° with reflection $|S_{11}|$ of less than -15 dB (Fig. 11(b)). Figure 11(c) indicates that the phase shift $|\Phi_{\max}|$, which yielded a 1-dB change in $\Delta|S_{21}|$, is 120° . Although the change in varactor diode reactance causes a resonant frequency shift in the unit element group, the effect on beam scanning performance is estimated to be small because the bandwidth of unit element group, at which $|S_{11}|$ is less than -15 dB, is more than 10%. The results in Fig. 11(b) indicate that this band is sufficiently wide for a 140° phase shift.

On the other hand, the conventional configuration causes significant changes in $|S_{11}|$ and $|S_{21}|$ and can change the phase by only 40° for $|S_{11}| < -15$ dB. This is because the varactor diodes are tuned over a wide DC-bias range and cause a loss in the low DC-voltage range. The reason $|S_{11}|$ changes is that the large change in the varactor diode impedance causes a serious reflection in the microstrip line. The results for the non-multi-stage configuration ($m = 1$) are similar to those of the conventional configuration, indicating a large reflection power and large attenuation in the transmitted power when Φ changes over a wide range. A minor improvement is observed compared with the conventional configuration. This is because the current in the varactor diodes is reduced in the $m = 1$ configuration because the diodes are attached to the antenna at positions where the current density is relatively small.

4. Verification of beam-scanning performance of MUSCAT array

This section presents the results of numerical analysis and experiments on an array having eight unit element groups to clarify the beam scanning performance of the MUSCAT array. **Figure 12** is a photograph of the fabricated MUSCAT array. The parameters of the unit element groups are the same as those in the previous section. The spacing of the units is set to be half the wavelength in vacuum and a termination load is attached to the end unit through the DC-block capacitor.

The calculated and measured radiation patterns of the MUSCAT array are shown in **Figs. 13(a)** and **(b)**. The calculated and measured values agreed except for the beamwidth even when the beam was steered.



Fig. 12. Fabricated antenna.

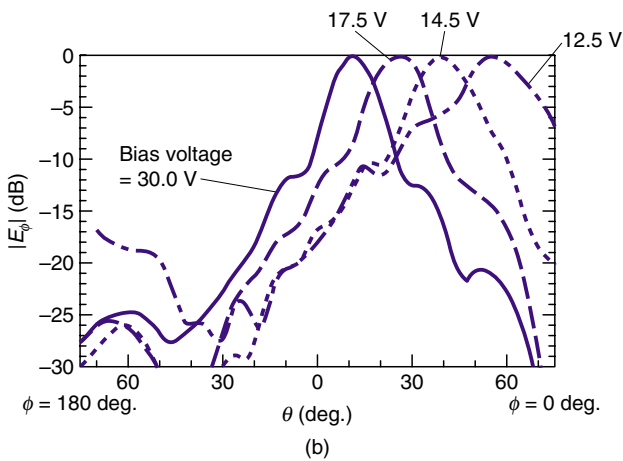
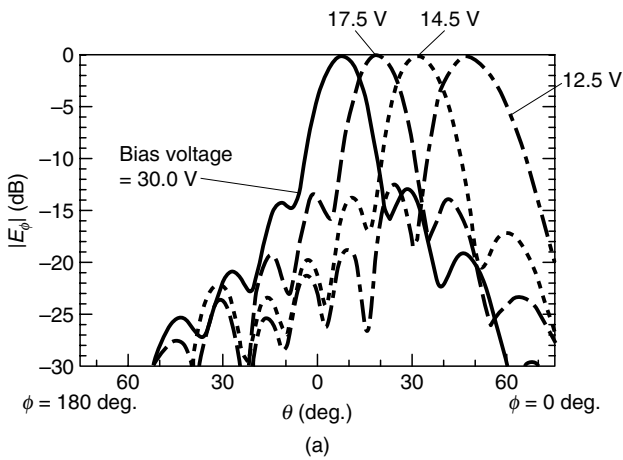


Fig. 13. Radiation pattern of MUSCAT array versus bias voltage: (a) calculated and (b) measured.

We did not find any large sidelobes or a mainlobe-split, which means that the traveling wave reflection at each unit element group is sufficiently small.

The $|S_{11}|$ and $|S_{21}|$ for the MUSCAT array are shown in Fig. 14. Here, f_c is the center frequency, which is

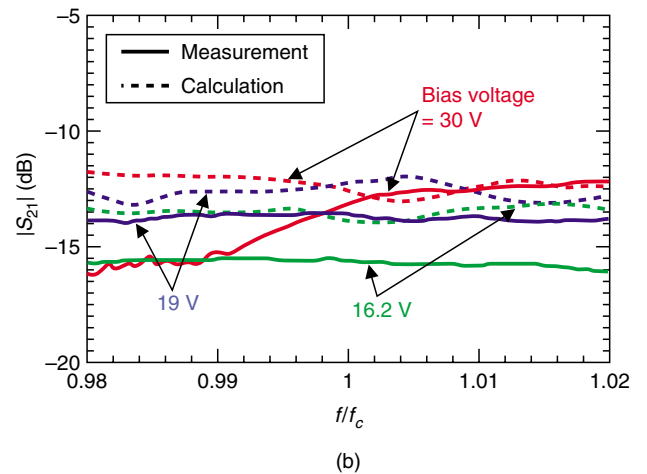
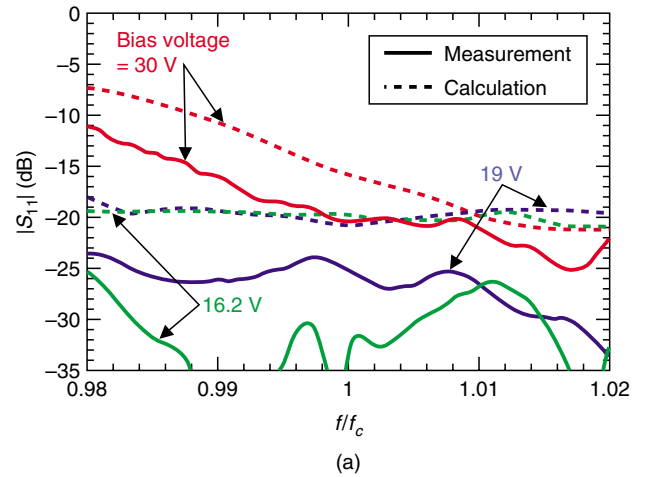


Fig. 14. $|S_{11}|$ and $|S_{21}|$ of MUSCAT array.

2.4 GHz. We observed that $|S_{11}|$ is less than -15 dB over 4% of the frequency range (f/f_c range from 0.98 to 1.02) except for 30 V. The measured $|S_{21}|$ is lower than the calculated value. From this result, we can understand why the measured beamwidth is wider

than the calculated beamwidth: it is because there is a steeper current-density distribution taper in the array in the measurement.

The actual gain versus the beam direction is shown in Fig. 15. The measured values agree well with the calculated ones and the range of the measured beam-scanning angle within a 3-dB decrease of the actual gain is approximately 27° . The measured beam direction shifts to the right because the reactance of the varactor diode has additional inductance due to the conductor line in the through hole shown in Fig. 2. The measured gain is almost the same as the calculated gain even for the difference in $|S_{21}|$ values between measurement and calculation shown in Fig. 14. From this result, we conjectured that the difference in $|S_{21}|$ is caused not by the loss, but by the radiation at the unit element group. On the other hand, the beam steering range of the non-multi-stage configuration ($m = 1$) is only 13° , and there is a serious gain reduction in the scanning range above 13° . When the same beam scanning angle is required for $m = 1$ and $m = 3$ configurations, the necessary phase shift for each element in the $m = 1$ configuration is much larger than that in the $m = 3$ configuration, and the lossy part of the tunable range in the varactor diode must be used in the $m = 1$ configuration. Moreover, the actual gain for $m = 1$ is always much less than that for $m = 3$ because the number of the antenna elements is fewer than that of $m = 3$ and the power consumed at the termination of $m = 1$ is large.

Since the proposed antenna has a symmetrical structure on the two sides of the center, the double range of the beam scanning can be obtained by exchanging the feed port and termination port.

Figure 16 shows the frequency dependence of the beam direction in the zx -plane and the gain in the MUSCAT array antenna. Here, both of these properties are normalized by f_c . The $\Delta\theta$ in Fig. 16(a) is the beam direction error from the beam direction at f_c . A negative $\Delta\theta$ value means that the beam direction is shifted in the direction of $\phi = 180^\circ$, and a positive $\Delta\theta$ value means it is shifted toward $\phi = 0$. We found that a beam direction error $\Delta\theta$ of $\pm 11^\circ$ occurred in the range of 4% bandwidth. Less than $\pm 5^\circ$ is seen in the range of 2% bandwidth. Because the width of the mainlobe is about 15° according to the radiation pattern in Fig. 13, the use of a 2% bandwidth for the fabricated MUSCAT array with eight unit element groups is adequate. If more bandwidth is required, fewer unit element groups should be used. Figure 16(b) shows the gain difference for the MUSCAT array: the gain difference within ± 3 dB is shown over

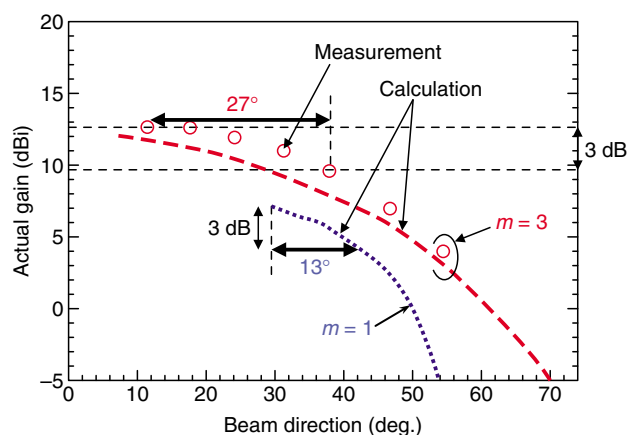


Fig. 15. Actual gain versus mainlobe direction.

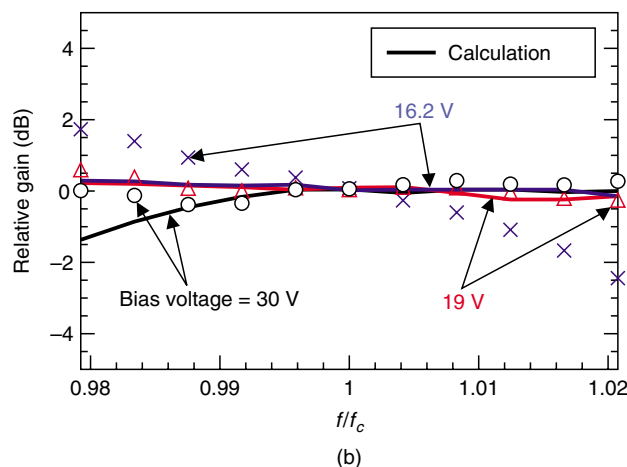
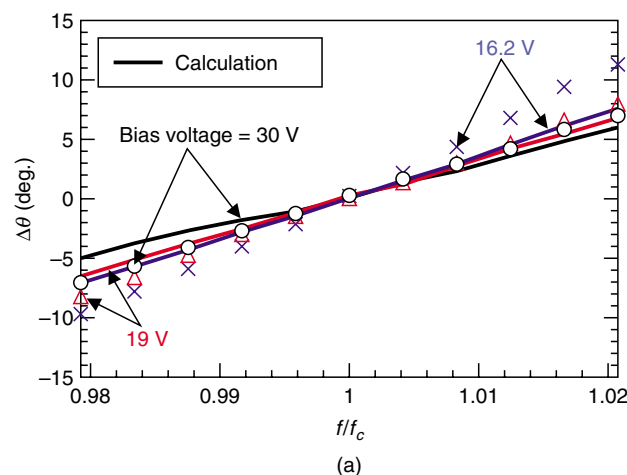


Fig. 16. Frequency dependence of radiation pattern: (a) beam direction error $\Delta\theta$ and (b) gain difference.

the range of a 4% bandwidth and that within only ± 1 dB is shown over the range of a 2% bandwidth.

The above results indicate that the proposed MUSCAT array can achieve easy operation and a wide beam scanning range with a simple geometry.

5. Conclusion

This paper proposed a MUSCAT array using unit element groups comprising multi-stage microstrip antennas with tunable reactance devices that achieves a wide beam scanning range with low loss and easy operation. We verified the performance of the unit element group, which consists of several microstrip antennas and is the basic element of the MUSCAT array. Numerical analysis of the unit element group showed that the multi-stage configuration of the unit element group extends the phase shift range to 120° , which is three times that of the conventional configuration in the range of 1-dB $|S_{21}|$ variation and yields more than 50% radiation efficiency for a configuration with three or more stages. We also found that the radiation pattern of the multi-stage configuration is almost the same as that of a single microstrip antenna.

We measured the radiation pattern of a fabricated MUSCAT array with eight unit element groups. This antenna achieved a wide range beam scanning of 27° , which is more than twice the beam scanning range of the non-multi-stage configuration. Since this antenna has a low-loss configuration, the discrete phase shifters with high insertion loss, which usually require low-noise amplifiers, are not necessary; that is, no complex bias control circuit is required. This design yields a simple and low-loss planar phased-array antenna that can be a key component of a low-profile satellite tracking system.

References

- [1] W. H. Jones and M. L. Chapelle, "Connexion by BoeingSM-broadband satellite communication system for mobile platforms," IEEE Military Communications Conference (MILCOM 2001.), Vol. 2, pp. 755-758, Oct. 2001.
- [2] F. Nagase, H. Tanaka, M. Nakayama, T. Seki, H. Kazama, and H. Mizuno, "Mobile multimedia satellite communication system," IEICE Trans. Commun., Vol. E84-B, No. 4, pp. 903-909, Apr. 2001.
- [3] J. R. James, G. D. Evans, and A. Fray, "Beam scanning microstrip arrays using diodes," IEE Proc. H, Vol. 140, No. 1, pp. 43-51, Feb. 1993.
- [4] N. Honma, F. Kira, T. Maruyama, K. Cho, and H. Mizuno, "Compact six-sector antenna employing patch Yagi-Uda array with common director," 2002 IEEE Antenna and Propagation Society International Symposium, Vol. 1, pp. 26-29, June 2002.
- [5] N. Honma, F. Kira, T. Maruyama, and K. Cho, "Compact planar four-sector antenna comprising patch Yagi-Uda arrays in a square configuration," 2002 IEEE Int. Symp. Antennas and Propagat. Soc. i-02, pp. 251-254, Nov. 2002.
- [6] <http://www.zeland.com/>
- [7] I. J. Bahl, "Build microstrip antennas with paper-thin dimensions," *Microwaves*, Vol. 18, pp. 50-63, Oct. 1979.



Naoki Honma

NTT Network Innovation Laboratories.
He received the B.E., M.E., and Ph.D. degrees in electrical engineering from Tohoku University, Sendai, Miyagi in 1996, 1998, and 2005, respectively. He joined NTT Radio Communication Systems Laboratories in 1998. He received the Young Engineers Award from the Institute of Electronics, Information and Communication Engineers (IEICE) of Japan in 2003 and the APMC Best Paper Award in 2003. His current research interest is planar antennas for high-speed wireless communication systems. He is a member of IEEE and IEICE.



Tomohiro Seki

Research Engineer, Wireless Systems Innovation Laboratory, NTT Network Innovation Laboratories.
He received the B.E. and M.E. degrees in electrical engineering from Tokyo University of Science, Tokyo in 1991 and 1993, respectively. In 1993, he joined NTT Radio Communication Systems Laboratories (now NTT Network Innovation Laboratories), Kanagawa. He has been engaged in the development of array antennas and active antennas for the millimeter-wave and microwave bands. He received the Young Engineer Award from IEICE in 1999. He is a member of IEEE and IEICE.



Koichi Tsunekawa

Senior Manager, Executive Research Engineer, Wireless Systems Innovation Laboratory, NTT Network Innovation Laboratories.
He received the B.S., M.S., and Ph.D. degrees in engineering science from the University of Tsukuba, Tsukuba, Ibaraki in 1981, 1983, and 1992, respectively. He joined the Electrical Communications Laboratories of Nippon Telegraph and Telephone Public Corporation (now NTT), Tokyo in 1983. Since 1984, he has been engaged in R&D of portable telephone antennas in land mobile communication systems. From 1993 to 2003, he was with NTT DoCoMo, Inc. where he worked on radio propagation research, intelligent antenna systems for wireless communications, and the development of IMT-2000 antenna systems. His research interests are antenna systems for MIMO transmission, millimeter-wave broadband access, and ubiquitous wireless system. He is a member of IEEE and IEICE.